Understanding Electrical and Optical Modulation Properties of Semiconductor Quantum-Dot Lasers in Terms of Their Turn-On Dynamics

Kathy Lüdge, Benjamin Lingnau, Christian Otto, and Eckehard Schöll
Institut für Theoretische Physik, Technische Universität Berlin, 10623 Berlin, GERRMANY
(Received 30 November, 2012)

The optical modulation properties of a semiconductor quantum-dot laser, as observed under optical injection, depend crucially on the internal carrier-carrier scattering processes within the device. In this paper we show that in order to predict the modulation properties of the laser it is most important to know the dynamics observed during the laser turn-on. In contrast to quantum-well lasers the turn-on damping of quantum-dot devices depends strongly nonlinear on the carrier-scattering lifetimes. Thus, different QD laser devices with internally scattering processes taking place on completely different time scales, can yield equal injection dynamics due to a qualitatively similar turn-on dynamics.

1. Introduction

Quantum-dot (QD) laser are multilayer semiconductor lasers where the inversion is reached within embedded zero dimensional structures that form in a self organized way during the growth process. The presence of both electrons and holes within the QDs allows for stimulated emission, and amplification of an electromagnetic field travelling inside the device. These QD lasers are promising candidates for telecommunication applications in optical fibers [1–4] due to their high temperature stability, their low value of the threshold current density and their emission wavelength around 1.3μm. Further these lasers show highly damped turn-on dynamics [5, 6] and, related to that, a low sensitivity to optical feedback [7–10].

To date the optical and electrical modulation properties of conventional quantum well lasers are fairly well understood [11],[12]. However, the dynamics of QD lasers under optical injection [13, 14] and electrical modulation [15, 16] remains in the focus of recent investigations. One reason for that is the additional dynamical degree of freedom within the device induced by the coupling of the zero-dimensional QDs to the surrounding

two-dimensional electron reservoir. For the case of optical injection, where a laser is unidirectionally coupled to an injecting master laser, QD lasers show smaller chaotic regions and less complicated trajectories compared to other laser devices [14]. The details of the locking behavior and the bifurcation structure sensitivity depends on the band structure and thus on the carrier-scattering lifetimes as shown in [13].

In this paper we want to show that the dependence of the optical modulation properties on the carrier lifetimes is strongly nonlinear and directly related to the turn-on damping rate of the laser. Since the turn-on damping shows a pronounced maximum for carrier-scattering lifetimes on the order of the relaxation oscillation (RO) frequency, as shown in [15], qualitatively similar turn-on dynamics of QD lasers can be found for either very small or very large lifetimes. Comparing the optical modulation properties for both cases allows to judge whether the details of the internal dynamics are crucial or whether the resulting turn-on dynamics suffices to predict the dynamic behavior under optical injection.

The structure of the paper is as follows. After introducing the model in Section 2 we discuss the turn-on dynamics of different QD lasers in

Section 3. Subsequently the electrical modulation properties as well as the dynamics with optical injection are presented in Section 4 and Section 5, respectively, both under the aspect of highlighting the role of the material model.
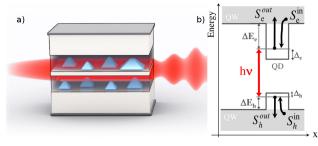

FIG. 1. (a) Scheme of the optically injected QD laser. QDs (light blue pyramids) are surrounded by a quantum well (QW) (b) Energy diagram of the band structure across a QD. $h\nu$ labels the ground state (GS) lasing energy. ΔE_e and ΔE_h mark the energetic distance of the GS from the QW band edge for electrons and holes, respectively. Δ_e and Δ_h denote the distance to the bottom of the QD confinement potential.

2. Model

The band structure of the QDs embedded in a quantum well laser structure is shown in Fig. 1. The confinement energies ΔE_e and ΔE_h mark the energy differences between the QD ground state and the band edge of the surrounding quantum well (QW) for electrons and holes, respectively. Our QD laser model is based on the model described in [5, 6] which has shown good quantitative agreement with experiments regarding the turn-on behavior and the modulation response of QD lasers [6].

For the modeling of the optical injection we use the ansatz already described [13] which is consistent with approaches made in [11, 17]. The set of six nonlinearly coupled rate equations displayed below describes the dynamics of the photon density n_{ph}, the phase of the electric field Φ, the electron and hole occupation probabilities in the QDs, ρ_e and ρ_h, and the electron and hole densities in the QW, w_e and w_h, respectively:

$$\dot{n}_{ph} = n_{ph}\left[2\bar{W}Z_a^{QD}(\rho_e+\rho_h-1)-2\kappa\right] + \frac{\beta}{A}2Z_a^{QD}R_{sp}(\rho_e,\rho_h) + \frac{2K}{\tau_{in}}\sqrt{n_{ph}n_{ph}^0}\cos(2\pi\Delta\nu_{inj}t-\Phi),\ (1)$$

$$\dot{\Phi} = \frac{\alpha}{2}\left[2\bar{W}Z_a^{QD}(\rho_e+\rho_h-1)-2\kappa\right] + \frac{K}{\tau_{in}}\sqrt{\frac{n_{ph}^0}{n_{ph}}}\sin(2\pi\Delta\nu_{inj}t-\Phi),\quad (2)$$

$$\dot{\rho}_e = -\bar{W}A(\rho_e+\rho_h-1)n_{ph}-R_{sp}(\rho_e,\rho_h)\quad + \quad S_e^{in}(w_e,w_h)(1-\rho_e)-S_e^{out}(w_e,w_h)\rho_e,\quad (3)$$

$$\dot{\rho}_h = -\bar{W}A(\rho_e+\rho_h-1)n_{ph}-R_{sp}(\rho_e,\rho_h)\quad + \quad S_h^{in}(w_e,w_h)(1-\rho_h)-S_h^{out}(w_e,w_h)\rho_h,\quad (4)$$

$$\dot{w}_e = \frac{j}{e_0}-2N^{QD}\left[S_e^{in}(1-\rho_e)-S_e^{out}\rho_e\right]-\tilde{R}_{sp},\quad (5)$$

$$\dot{w}_h = \frac{j}{e_0}-2N^{QD}\left[S_h^{in}(1-\rho_h)-S_h^{out}\rho_h\right]-\tilde{R}_{sp}.\quad (6)$$

Here, $\bar{W}$ is the Einstein coefficient for the coherent interaction and $Z_a^{QD}=a_LAN_a^{QD}$ is the number of active QDs inside the waveguide (the factor 2 accounts for the spin degeneracy of the QD levels). a_L is the number of self-organized QD layers and A is their in-plane area. N_a^{QD} is the density of dots per unit area of the active QDs. As a result of the size distribution and material composition fluctuations of the QDs the gain spectrum is inhomogeneously broadened,

and only a subgroup (density N_a^{QD}) of all QDs (N^{QD}) matches the mode energies for lasing. The spontaneous emission from one QD is taken into account by $R_{sp}(\rho_e, \rho_h) = W\rho_e\rho_h$, where W is the Einstein coefficient for spontaneous emission resulting from incoherent interaction of the QD with all resonator modes. Please note that the coefficients $\bar{W}$ and W differ by three orders of magnitude, and see e.g. [13] for details on their derivation. β is the spontaneous emission factor, measuring the probability that a spontaneously emitted photon is emitted into the lasing mode. Losses in the QW are taken into account by $\tilde{R}_{sp} = B^S w_e w_h$. 2κ are the optical intensity losses. n_{inj} is the injected photon density in the active region of the QD laser per cavity round trip time and $\Delta\nu_{inj} = \nu_{inj} - \nu_L$ is the input detuning between the injecting laser frequency and the frequency of the solitary QD laser. The time τ_{in} for one roundtrip of the light in the cavity of length L is given by $\tau_{in} = 2L\sqrt{\varepsilon_{bg}}/c$ with background permittivity ε_{bg}. n_{ph}^0 designates the steady state photon density without injection ($K = 0$) which of course depends on all operation parameters.

The linewidth enhancement factor α in Eq. (2) models the phase-amplitude coupling of the electric field $E \sim \sqrt{n_{ph}}e^{i\phi}$. For QD lasers this quantity α is problematic as discussed recently [18], because it cannot account for the independent dynamics of resonant (ρ_e, ρ_h) and nonresonant (w_e, w_h) charge carriers [18–20] and eventually neglects a degree of freedom of the dynamics. It was, however, shown that QD laser models based on an α parameter still yield reliable results as long as only the transitions between stable and unstable behavior, i.e., Hopf and saddle-node bifurcations, are investigated [18, 20]. Since this is the focus of our paper we choose α to be constant but keep in mind that it may vary with the operation conditions and that more complex bifurcation scenarios may be missed.

The in- and out-scattering rates for electrons and holes between QD and QW are denoted by S_e^{in}, S_e^{out} and S_h^{in}, S_h^{out} as depicted in Fig. 1. They result from microscopic calculations of the Coulomb interaction between the 2D

Table 1. Numerical parameters used in the simulation unless stated otherwise

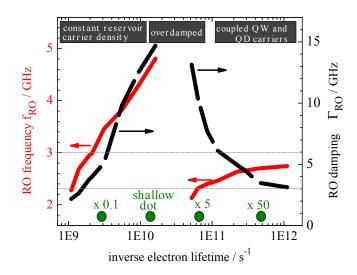| symbol	value	symbol	value
W	$0.44ns^{-1}$	A	$4 \cdot 10^{-5} cm^2$
$\bar{W}$	$0.33\mu s^{-1}$	N_a^{QD}	$2.7 \cdot 10^{10} cm^{-2}$
2κ	$0.1ps^{-1}$	N^{QD}	$1 \cdot 10^{11} cm^{-2}$
β	$2.2 \cdot 10^{-3}$	B^S	$500ns^{-1}nm^2$
a_L	15	τ_{in}	$24ps$
Z_a^{QD}	$1.8 \cdot 10^6$	α	0.9
T	$300K$	$\Delta E_e(\Delta E_h)$	$74meV$ $(40meV)$

FIG. 2. Turn-on damping Γ_{RO} and relaxation oscillation frequency f_{RO} of a QD laser with different internal steady state scattering lifetimes. The green circles denote the different QD lasers discussed in the following. The pump current is set to $j = 2j_{th}$ (note that the threshold current j_{th} changes with τ)

carrier reservoir and the zero dimensional QD (please note that in- and out scattering rates are connected by detailed balance [5, 21]). The microscopically calculated carrier scattering rates used here are documented in [13]. They depend on the carrier densities in the carrier reservoir and on the band structure of the device. In contrast to our previous paper [13] where we concentrated on the impact of the band structure on the turn-on dynamics and the locking behavior, the focus of the present work is to resolve the role of the material model for the modulation properties by comparing QD lasers with equal turn-on

parameters but different internal dynamics. This is possible because the turn-on damping Γ_{RO} as well as the turn-on frequency f_{RO} depend in a strongly nonlinear manner upon the scattering lifetimes (defined by $\tau_{e,h} = (S_{e,h}^{in} + S_{e,h}^{out})^{-1}$) as can be seen in Fig. 2. Consequently a QD laser can have similar values of Γ_{RO} for completely different carrier scattering mechanisms. The green circles in Fig. 2 mark the different QD lasers studied in the following. They are chosen to cover all three different dynamical regimes introduced in [15], namely the "constant reservoir carrier density regime" left of the maximum RO damping found for slow scattering rates, the "coupled regime" around the maximum and the regime of "synchronized QD and QW dynamics" found for very high scattering rates.

3. Turn-on dynamics

We start our discussion by considering the shallow quantum dot laser with one ground state as shown Fig. 1. The steady state lifetimes of this laser are $\tau_e = 62\,ps, \tau_h = 15\,ps$ for a current of $j = 2j_{th}$ and therefore this laser lies in the intermediate regime left of the overdamped regime of Fig. 2 and shows strongly damped turn-on dynamics. Its turn-on transients for different pump currents j are plotted in Fig. 3b. By either decreasing or increasing the carrier lifetimes of this shallow QD laser by an order of magnitude we find reappearing oscillations in the turn-on as can be seen in Fig. 3a and c. Experimentally this variations in the carrier lifetimes can be achieved by the presence of excited states, by different dot size (different confinement energies) or by variations in the device temperature. However for our purpose we simply use the microscopic rates of the shallow dot laser and multiply them by a factor of 0.1 (Fig. 3a) and 50 (Fig. 3c), respectively. Please note that the QD laser considered here has a much higher gain coefficient $g \sim 2Z_a^{QD}\bar{W}$ if compared to the laser modeled in [13]. The reason is that in the present paper a much higher percentage (30%) of

the inhomogeneously broadened QD ensemble is actually participating in the lasing process. Thus, although equal functions for the microscopic rates of the shallow QD are used, the steady states of all carrier densities vary with the gain leading to different turn-on transients and later on also to different injection locking behavior.

For a better comparison the turn-on dynamics for the different lasers have been fitted with a damped sinusoidal function. The results for f_{RO} and Γ_{RO} are displayed in Fig. 3d and e, respectively, as a function of multiples of the respective threshold current j_{th}. The dependence of f_{RO} and Γ_{RO} on the electrical pump current j depends on the different timescales embedded in the dynamic equations (1)-(6). For the case of slow scattering rates (shallow dot× 0.1) analytic equations, published in a previous publication [22], exist. They read:

$$2\pi f_{\times 0.1}^{RO} = \sqrt{4\kappa \bar{W} A n_{ph}^*},\qquad(7)$$

$$\Gamma_{\times 0.1}^{RO} = \frac{W}{2}\left[1 + \frac{2\kappa}{2Z_a^{QD}\bar{W}}\right] + \bar{W}A n_{ph}^*$$
$$+ \frac{1}{4}\left[\frac{1}{\tau_e^*} + \frac{1}{\tau_h^*}\right].\qquad(8)$$

The values resulting from Eqs. (7) and (8), using the steady state values n_{ph}^*, τ_h^* and τ_e^* obtained from numeric integration, are plotted as dashed green line in Fig. 3d and e and match nicely with the results obtained by fitting the turn-on dynamics. However, Eqs. (7) and (8) break down for the case of the very fast rates (shallow dot ×50), as for this case different scalings have to be used in the asymptotic derivation.

The nearly instantaneous coupling between the QDs and the reservoir leads to turn-on dynamics that are not mainly determined by the carrier scattering lifetimes between QW and QD but by the photon lifetime and the carrier losses inside the QW (as known for QW lasers). In the limit $\tau_e\omega^{RO} \ll 1$ the rate equation system can be reduced by using a steady state relation for $\rho_e(w_e)$ and $\rho_h(w_e)$ which can be derived from $\dot{\rho}_e = \dot{\rho}_h = 0$. In this limit of instantaneous
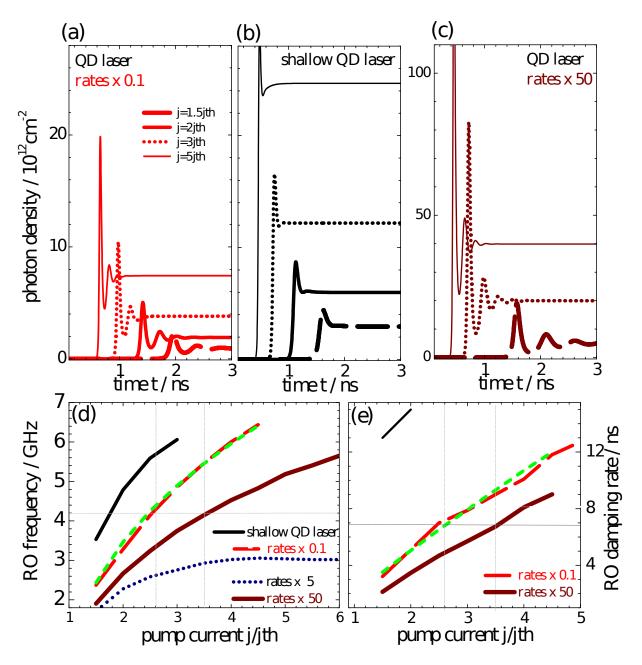
FIG. 3. Turn-on oscillations for QD lasers with three different internal carrier-scattering lifetimes: (a)10-fold slower rates than microscopically calculated, (b) rates as obtained for shallow dot QD laser, (c) 50-fold faster rates. The pump current varies between $j = 1.5j_{th}$ and $j = 5j_{th}$ (note that the threshold current changes with τ) (d) and (e) show the RO frequency and damping rates, respectively, in terms of the pump current as obtained by fitting the turn-on dynamics plotted above close to the fixed point. Green dashed lines: Analytic results for 10-fold slower rates given by Eqs.(7),(8)

coupling between QW and QD the dynamics is described by 2 dynamic variables (w_e and ρ_e) and $f_{\tau_e \to 0}^{RO}$ and $\Gamma_{\tau_e \to 0}^{RO}$ can be obtained analytically

from linearizing the reduced rate equation system around the steady state. The equations read:

$$2\pi f^{RO}_{\tau_e \to 0} = \sqrt{4\kappa \bar{W} A n^*_{ph}} \sqrt{\frac{\partial(\rho_e + \rho_h)}{\partial(w_e/N^{QD})}}, \qquad (9)$$

$$\Gamma^{RO}_{\tau_e \to 0} = \frac{1}{2}$$

$$\times \left[2\bar{W} A n^*_{ph} \frac{\partial(\rho_e + \rho_h)}{\partial(w_e/N^{QD})} + B^S(w^*_h + w^*_e) \right] \qquad (10)$$

The values resulting from Eqs. (9) and (10) are plotted as horizontal lines in Fig. 2 and describe nicely the limits of f^{RO} and Γ^{RO} if $\tau_e \to 0$. Further the appearance of the derivative $\frac{\partial(\rho_e + \rho_h)}{\partial(w_e/N^{QD})} \approx 0.15$ in Eq.(9) underlines that reappearing RO oscillations in the coupled regime can only be found if the ratio between in- and out scattering rates depends on the carrier density in the reservoir. Otherwise the derivative of $\rho_{e,h}$ which is in this limit given by $\rho_{e,h} = (1 + S^{out}_{e,h}/S^{in}_{e,h})^{-1}$ vanishes.

The idea now is to compare the modulation properties for lasers with equal turn-on frequency f_{RO} and damping Γ_{RO} in order to single out the impact of the material model. As indicated by the thin horizontal lines in Fig. 3(d) and (e) the two lasers ($\times 50$ and $\times 0.1$) have equal turn-on parameters for the currents: $j^{\times 0.1} = 2.6 j_{th}$ and $j^{\times 50} = 3.5 j_{th}$. The original shallow dot laser has equal RO frequency at $j^{\times 1} = 2 j_{th}$ however its damping is much higher as can be seen in Fig. 3b.

4. Electrical modulation response

The electrical modulation response of the different lasers which have been discussed above is plotted in Fig. 4a. The pump currents were chosen to yield equal f_{RO} for the different lasers (see horizontal line in Fig. 3d) . To obtain the results, the laser was operated without optical injection ($K = 0$) but with an electric pump current that was modulated by a small amplitude sinusoidal signal. The response curves of the different QD lasers (different internal scattering
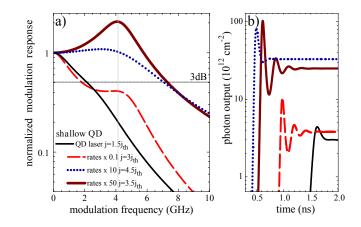

FIG. 4. (a) Electrical modulation response of a quantum dot laser and (b) corresponding turn-on dynamics with the different internal scattering lifetimes already used in Fig. 3. The pump current was chosen to yield equal RO frequency for all 4 lasers (see thin horizontal line in Fig. 3d).

lifetimes) appear to be very different. For the very fast rates a pronounced resonance peak at the turn-on frequency f_{RO} is found (solid brown curve), while the QD laser with very slow rates (red dashed curve) shows a strongly decreasing response curve which is similar to the response of the shallow QD laser for modulation frequencies below $3GHz$. Nevertheless there is a resonance peak for the slow carrier dynamics but it appears much below the 3dB mark.

The explanation can be given by looking at the internal timescales. While the fast scattering processes (shallow dot $\times 50$) result in an enslavement of the QD population leading to a response curve as known from QW lasers, given by $H(\omega) = \frac{\omega_0^4}{(\omega_0^2 - \omega^2)^2 + 4\Gamma_{RO}^2 \omega^2}$ with $\omega_0^2 \approx \omega_{RO}^2 + \Gamma_{RO}^2$. The slow scattering between QD and reservoir (shallow dot and shallow dot $\times 0.1$), on the other hand, leads to an additional degree of freedom in the dynamics and thus additional effects in the response function. For this regime the relatively slow dynamics of the carrier transfer between QD and QW becomes important for the electrical modulation properties and the transfer function for the modulation response has an additional decaying contribution. This effect
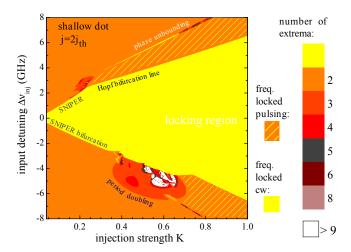
FIG. 5. Two-parameter bifurcation diagram of the shallow-dot QD laser introduced above. Colored shading labels the number of maxima found in the time series per period, and the yellow shading shows the region of cw laser emission (locking tongue).

was also recently reported in [15, 16]. Thus, as soon as the carrier scattering times are on a timescale larger than the inverse RO frequency, a modified transfer function needs to be used for the electric modulation response that deviates from the commonly known simple function.

However, although two of these different lasers yield equal RO frequency and damping, evaluating the turn-on delay time allows one to distinguish the internal carrier lifetimes as can be seen in Fig. 4b. The delay time as well as the photon density is much larger for the slow carrier dynamics between QD and QW. This effect can be understood analytically as reported in [23].

5. Laser dynamics under optical injection

If the laser is subjected to external optical injection a variety of different dynamics can be found in its time dependent output intensity as described in detail in [11, 13]. It strongly depends on the input laser frequency $\Delta\nu_{inj}$ as well as on its intensity K. This parameter dependence can be best visualized in a two-parameter bifurcation

diagram where qualitatively different behavior is indicated by different shading. The results obtained by direct integration are summarized as a contour plot showing locking tongues as known from the Adler-equation [24]. These tongues are the yellow regions in Fig. 5 and they represent the parameter domain where the slave laser is forced to emit continuous waves (cw) at the same frequency as the injecting master laser. Outside the yellow region the slave laser emits light that is modulated in time showing 2 (orange area), 4(red area) or more, different maxima per period. The transition from the yellow locking region to the pulsating solutions is formed either by a Hopf bifurcation or a by a saddle node bifurcation on a limit cycle (SNIPER) as indicated in Fig. 5. Within the yellow hatched area the frequency of the modulated light is still locked to the master frequency.

As a result of the discussions presented in the last section it is known that both the RO damping and frequency depend crucially on the pump current. Thus it is expected that changing the pump current leads to changes in the locking behavior of the injected laser. This can be seen in Fig. 6. Here the results for a shallow dot laser with rates increased by a factor of 5 are shown for a current of $j = 3.5j_{th}$ and $j = 5j_{th}$. Note that this laser shows qualitatively similar turn-on dynamics as the shallow dot laser of Fig. 5a, but with a RO frequency that is much smaller. The dashed vertical lines in Fig. 6 mark the three major changes of the bifurcation diagram with the current. At first the saddle-node-Hopf point, i.e. the point in parameter space where the Hopf bifurcation line meets the saddle-node (SNIPER) bifurcation line as the border of the locking tongue at the positive detuning side, shifts to higher injection strength K. This effect was also observed in [13] and can be attributed to an increase in the RO damping Γ_{RO}. Second, the position of the period doubling loop at the negative detuning side shifts to higher K with increasing j, and last but not least the width of the period doubling loop changes. Comparing results for equal damping but different
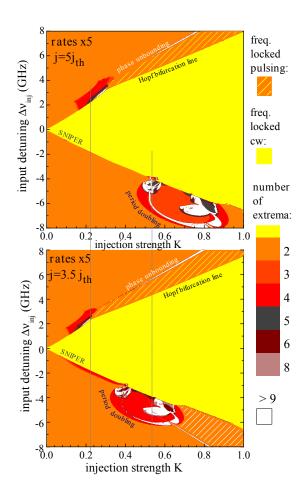
FIG. 6. Locking tongues of a shallow-dot QD laser with 5-fold faster rates for two different electrical pump currents $j = 3.5j_{th}$ and $j = 5j_{th}$. Colored shading labels the number of maxima found in the time series per period, and yellow shading shows the locking region.

FIG. 7. Locking tongues of two QD lasers with different internal scattering lifetimes ($\times 0.1$ and $\times 50$) at a pump current of $j = 2j_{th}$. Colored shading labels the number of maxima found in the time series per period, and yellow shading shows the locking region.

RO frequency (not shown here) show that the width of the period doubling loop indeed increases with the RO frequency.

To elucidate the impact of the internal processes we now compare the injection dynamics for two QD lasers that show turn-on dynamics with equal RO frequency and damping but that have different carrier lifetimes. To reach this goal we use two QD lasers left and right of the overdamped region in Fig. 2 (scattering rates $\times 50$ and $\times 0.1$) and operate them with different pump currents j (see Fig. 3 for the dependence of f_{RO} and Γ_{RO} on j). At first it is obvious that these
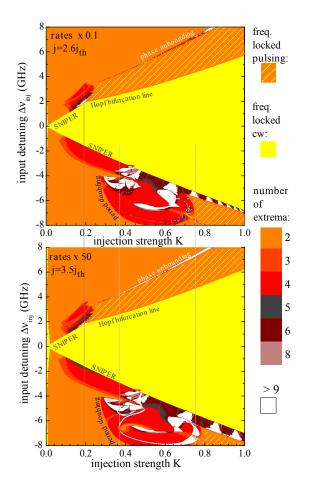
two lasers are much more sensitive to external perturbations and thus show a more complicated bifurcation diagram than the original shallow dot laser of Fig. 5. As can be seen in Fig. 7, the saddle-node-Hopf point as well as the position of the period-doubling regime are equal for the two weakly damped QD lasers. However, the exact shape of the period-doubling regime depends on the internal processes, which are different in both cases (the scattering rates differ by 3 orders of magnitude).

6.   Conclusion

We have shown that in order to predict the optical modulation properties of a QD laser it is most important to know the dynamics observed during the laser turn-on. Different QD laser devices with internal scattering processes taking place on completely different time scales can yield equal injection dynamics if they yield qualitatively similar turn-on dynamics. However, the electrical modulation properties depend on all internal carrier-scattering timescales.

These results are important in conjunction with possible model reductions. That is, in order to predict the turn-on dynamics of a QD laser over a range of different operating conditions it is crucial to microscopically include the complete set of nonlinear internal scattering processes. However, for describing optical injection or feedback experiments with a QD laser where the turn-on dynamics is known, it is possible to significantly reduce the model.

Acknowledgment

References

[1] D. Bimberg: *Quantum dots for lasers, amplifiers and computing*, J. Phys. D **38**, 2055 (2005).

[2] D. Bimberg, M. Grundmann, and N. N. Ledentsov: *Quantum Dot Heterostructures* (John Wiley & Sons Ltd., New York, 1999).

[3] E. U. Rafailov, M. A. Cataluna, and E. A. Avrutin: *Ultrafast Lasers Based on Quantum Dot Structures* (WILEY-VCH, Weinheim, 2011).

[4] K. Lüdge: *Nonlinear Laser Dynamics - From Quantum Dots to Cryptography* (Wiley-VCH, Weinheim, 2012).

[5] K. Lüdge and E. Schöll: *Quantum-dot lasers – desynchronized nonlinear dynamics of electrons and holes*, IEEE J. Quantum Electron. **45**, 1396 (2009).

[6] K. Lüdge, R. Aust, G. Fiol, M. Stubenrauch, D. Arsenijević, D. Bimberg, and E. Schöll: *Large signal response of semiconductor quantum-dot lasers*, IEEE J. Quantum Electron. **46**, 1755 (2010).

[7] G. Huyet, D. O'Brien, S. P. Hegarty, J. G. McInerney, A. V. Uskov, D. Bimberg, C. Ribbat, V. M. Ustinov, A. E. Zhukov, S. S. Mikhrin, A. R. Kovsh, J. K. White, K. Hinzer, and A. J. SpringThorpe: *Quantum dot semiconductor lasers with optical feedback*, phys. stat. sol. (b) **201**, 345 (2004).

[8] C. Otto, K. Lüdge, and E. Schöll: *Modeling quantum dot lasers with optical feedback: sensitivity of bifurcation scenarios*, phys. stat.

sol. (b) **247**, 829 (2010).

[9] C. Otto, K. Lüdge, E. A. Viktorov, and T. Erneux: *Quantum dot laser tolerance to optical feedback*, in *Nonlinear Laser Dynamics - From Quantum Dots to Cryptography*, edited by K. Lüdge (WILEY-VCH, Weinheim, 2011), chap. 6, pp. 141–162.

[10] B. Globisch, C. Otto, E. Schöll, and K. Lüdge: *Influence of carrier lifetimes on the dynamical behavior of quantum-dot lasers subject to optical feedback*, Phys. Rev. E **86**, 046201 (2012).

[11] S. Wieczorek, B. Krauskopf, T. Simpson, and D. Lenstra: *The dynamical complexity of optically injected semiconductor lasers*, Phys. Rep. **416**, 1 (2005).

[12] L. A. Coldren and S. W. Corzine: *Diode Lasers and Photonic Integrated Circuits* (John Wiley and Sons, New York, 1995).

[13] J. Pausch, C. Otto, E. Tylaite, N. Majer, E. Schöll, and K. Lüdge: *Optically injected quantum dot lasers - impact of nonlinear carrier lifetimes on frequency locking dynamics*, New J. Phys. **14**, 053018 (2012).

[14] B. Kelleher, C. Bonatto, G. Huyet, and S. P. Hegarty: *Excitability in optically injected semiconductor lasers: Contrasting quantum-well- and quantum-dot-based devices*, Phys. Rev. E **83**, 026207 (2011).

[15] B. Lingnau, K. Lüdge, W. W. Chow, and E. Schöll: *Influencing modulation properties of*

quantum-dot semiconductor lasers by electron lifetime engineering, Appl. Phys. Lett. **101**, 131107 (2012).

[16] C. Wang, F. Grillot, and J. Even: *Impacts of wetting layer and exciter state on the modulation response of quantum-dot lasers*, IEEE J. Quantum Electron. **48**, 1144 (2012).

[17] G. H. M. van Tartwijk and D. Lenstra: *Semiconductor laser with optical injection and feedback*, Quantum Semiclass. Opt. **7**, 87 (1995).

[18] B. Lingnau, K. Lüdge, W. W. Chow, and E. Schöll: *Failure of the α-factor in describing QD laser dynamical instabilities and chaos*, Phys. Rev. Lett. (2012), submitted, arXiv:1210.5413.

[19] S. Melnik, G. Huyet, and A. V. Uskov: *The linewidth enhancement factor α of quantum dot semiconductor lasers*, Opt. Express **14**, 2950 (2006).

[20] B. Lingnau, K. Lüdge, W. W. Chow, and E. Schöll: *Many-body effects and self-contained phase dynamics in an optically injected quantum-dot laser*, in *Semiconductor Lasers and Laser Dynamics V, Brussels*, edited by K. Panajotov, M. Sciamanna, A. A. Valle, and R. Michalzik (SPIE, 2012), vol. 8432 of *Proceedings of SPIE*, pp. 84 321J–1.

[21] K. Lüdge and E. Schöll: *Nonlinear dynamics of doped semiconductor quantum dot lasers*, Eur. Phys. J. D **58**, 167 (2010).

[22] K. Lüdge, E. Schöll, E. A. Viktorov, and T. Erneux: *Analytic approach to modulation properties of quantum dot lasers*, J. Appl. Phys. **109**, 103112 (2011).

[23] G. S. Sokolovskii, V. V. Dudelev, E. D. Kolykhalova, A. G. Deryagin, M. V. Maximov, A. M. Nadtochiy, V. I. Kuchinskii, S. S. Mikhrin, D. A. Livshits, E. A. Viktorov, and T. Erneux: *Nonvanishing turn-on delay in quantum dot lasers*, Appl. Phys. Lett. **100**, 081109 (2012).

[24] R. Adler: *A Study of Locking Phenomena in Oscillators*, IRE **34**, 351 (1946).